Chemical Science

ROYAL SOCIETY OF CHEMISTRY

EDGE ARTICLE

View Article Online
View Journal | View Issue



Cite this: *Chem. Sci.*, 2025, **16**, 23220

All publication charges for this article have been paid for by the Royal Society of Chemistry



# DiICz MR-TADF emitters as potent energy transfer photocatalysts

Lea Hämmerling, David Hall, Eliott Blin, Tabea Heil and Eli Zysman-Colman *

Photoinduced energy transfer (PEnT) reactions are a subset of photochemical reactions that involve the indirect photoactivation of substrates following an energy transfer from a photoexcited sensitizer/photocatalyst. Examples of PEnT reactions include *E*/*Z* isomerizations, [2 + 2] cycloadditions, and sigmatropic shifts. Here we introduce a family of diindolocarbazole (DiICz) multi-resonant thermally activated delayed fluorescent (MR-TADF) photocatalysts (PCs), **DiICztBu$_4$**, **DiICzMes$_4$**, **DiICztBuCz$_4$**, and **DiICztBuDPA$_4$**, which have relatively high triplet energies ($E_T$). We cross-compare their photocatalytic behavior and that of relevant literature reference PCs' in five distinct PEnT reactions. We demonstrate that the use of the DiICz PCs consistently leads to more rapid reaction rates and higher yields compared to the widely used **4CzIPN**. **DiICztBu$_4$**, **DiICzMes$_4$**, and **DiICztBuCz$_4$** possess similar $E_T$ but decreasing singlet–triplet energy gaps, $\Delta E_{ST}$, enabling for the first time a comparison of the dependency of both the reaction kinetics and the final yield on this photophysical parameter. We observed that when the reaction kinetics are fast, there is little sensitivity to quenching of the excited PC by oxygen, implying that Dexter Energy Transfer (DET) to the substrate is competitive with DET to oxygen. Importantly, this means that some of the DET reactions using these PCs can be performed in air without adversely affecting reaction yield.

Received 3rd June 2025
Accepted 27th October 2025

DOI: 10.1039/d5sc04014k

rsc.li/chemical-science

## Introduction

One major class of photochemical reactions consists of those that proceed *via* a photoinduced energy transfer (PEnT) mechanism, which typically involves an electronically excited photocatalyst (PC*) transferring its energy to a substrate (sub). The substrate in its electronically excited state (sub*) then undergoes a photochemical transformation.[1–3] The majority of PEnT reactions proceed *via* Dexter Energy Transfer (DET) reactions. DET involves the simultaneous double electron exchange between the PC* and the sub to generate a PC in its $S_0$ state and a sub*. This can take place from the singlet state of the $^1$PC* to generate $^1$sub* or more commonly from the triplet state of $^3$PC* to generate $^3$sub* (Fig. S1) and does not involve a change in the overall multiplicity.[1] DET processes occur over shorter distances, typically less than 10 Å,[4] as orbital overlap between the PC and the sub is required, which implies a collisional interaction is needed for DET to occur intermolecularly.

In cases where DET occurs from the $^3$PC* to $^3$sub, it is the spectral overlap of the phosphorescence of the $^3$PC* and the spin-forbidden absorption of the substrate that is relevant to generate $^3$sub*. Notably, as the spin-forbidden absorption spectrum is of negligible intensity in most organic substrates, the low-energy onset of the low-temperature phosphorescence spectrum of the sub is used as a surrogate estimation of the energy at which spectral overlap no longer occurs, which is none other than the energy of the $T_1$ state ($E_T$) of the sub. It is generally accepted that DET will occur when $E_T$(PC*) > $E_T$(sub*), and the closer these two values are, the more likely DET is to occur.[5] Given that the $^3$sub* has a biradical-like character, this enables a diversity of reactions such as *E*/*Z* isomerization,[2,6–8] cycloadditions such as [2 + 2],[9–11] sensitization of metal complexes,[12–14] homolytic bond cleavages such as $N_2$ release from benzoyl azides, scission of S–S bonds, and N–O dissociation of oxime esters to instigate the formation of carbon-centered and nitrogen-centered radicals in concert with the loss of $CO_2$.[15–17]

Of the PCs typically employed in PEnT reactions, organic carbonyl-based photosensitizers have the highest $E_T$. For instance, xanthone and acetophenone (Fig. 1) have similar $E_T$ values of 3.22 eV (74.2 kcal mol$^{-1}$, 310.5 kJ mol$^{-1}$) and 3.21 eV (74.0 kcal mol$^{-1}$, 309.6 kJ mol$^{-1}$).[1,2,18] Organometallic PCs are particularly popular for PEnT reactions in part because the presence of the heavy metal center ensures an essentially quantitative triplet yield as a result of fast intersystem crossing (ISC) mediated by its large spin–orbit coupling (SOC).[19,20] Two of the most commonly used organometallic PCs for PEnT reactions include **[Ir(dF(CF$_3$)ppy)$_2$(dtbbpy)](PF$_6$)** ($E_T$ = 2.68 eV)[5] for

*Organic Semiconductor Centre, EaStCHEM School of Chemistry, University of St Andrews, St Andrews, KY16 9ST, UK. E-mail: eli.zysman-colman@st-andrews.ac.uk*

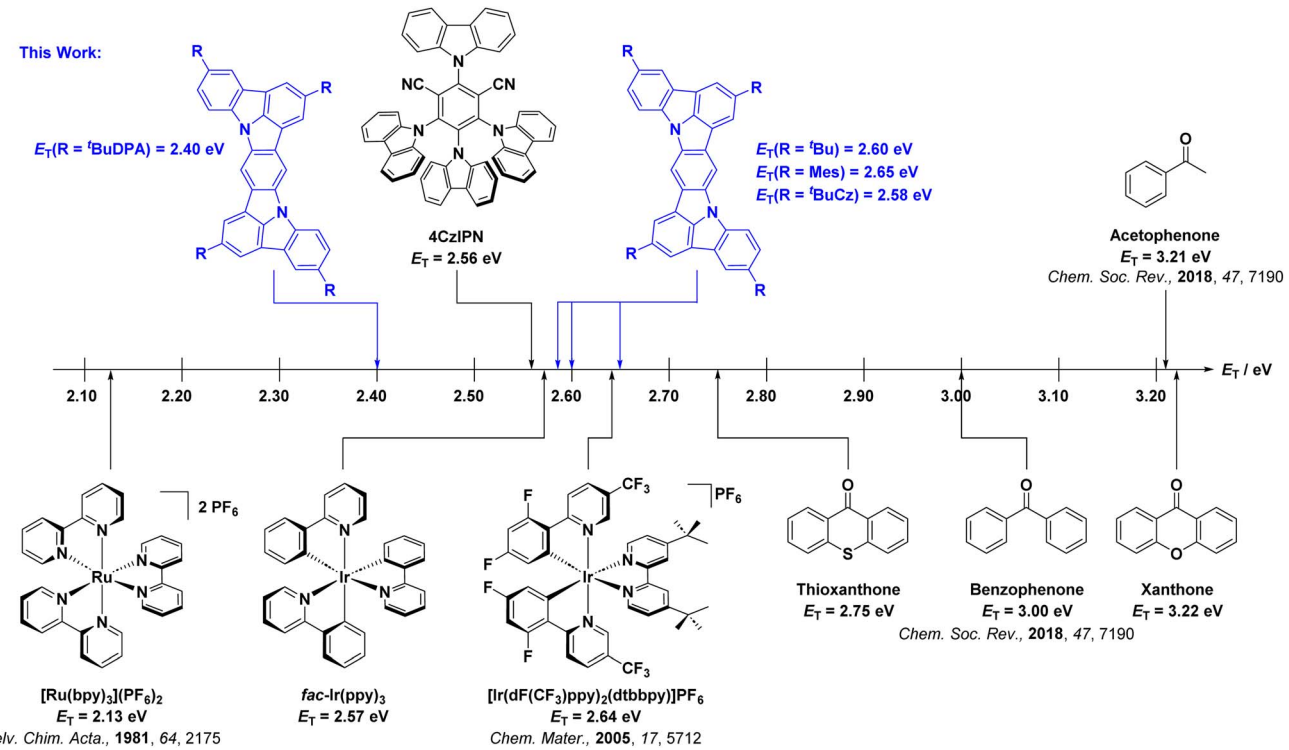


Fig. 1 Chemical structures and $E_T$ for selected literature PCs used for DET reactions and for the four TADF PCs investigated in this work. Quoted $E_T$ values for **4CzIPN**, **DiICztBu$_4$**, **DiICzMes$_4$**, **DiICztBuCz$_4$** and **DiICztBuDPA$_4$** were estimated from $E_T = E_S - \Delta E_{ST}$, with $E_S$ being the onset of the steady-state emission in DCM at room temperature and $\Delta E_{ST}$ determined in 2-MeTHF glass at 77 K. $E_T$ for ***fac*-Ir(ppy)$_3$** was taken from the onset of the room temperature emission in 2-MeTHF. $E_T$ for **[Ru(bpy)$_3$](PF$_6$)$_2$** was taken from the emission maximum at 77 K in 4 : 1 MeOH/EtOH glass.[22] $E_T$ for **[Ir(dF(CF$_3$)ppy)$_2$(dtbbpy)]PF$_6$** was taken from the room temperature emission maximum in MeCN.[23] For the organic PCs, $E_T$ is measured from the phosphorescence spectra at 77 K.[5]

reactions requiring a relatively high $E_T$ and **[Ru(bpy)$_3$](PF$_6$)$_2$** ($E_T$ = 2.12 eV)[21] for those that do not (Fig. 1).

Over the last decade or so, organic thermally activated delayed fluorescence (TADF) compounds have been increasingly used in the academic community as alternatives to organometallic complexes, initially as emissive materials for organic light-emitting diodes (OLEDs),[24] and later, as PCs.[25,26] This is because TADF compounds have accessible triplet states owing to the small energy gap ($\Delta E_{ST}$) between their lowest excited singlet ($S_1$) and triplet ($T_1$) states, which allows for relatively fast ISC and reverse ISC (RISC) to take place, despite the small SOC between these states in the absence of heavy atoms.[27,28] Molecules with small $\Delta E_{ST}$ are those where the donor (D) and acceptor (A) moieties are sufficiently electronically decoupled such that there is minimal orbital overlap between the highest occupied molecular orbital (HOMO) and the lowest unoccupied molecular orbital (LUMO), *i.e.*, the exchange energy is small. This spatial separation also produces an emissive excited state having charge transfer (CT) character. The most widely employed molecular design is one that adopts a strongly twisted D–A structure, exemplified in **4CzIPN** and **4DPAIPN** (Fig. S2).[26] Owing to the distance between D and A units, the emissive $S_1$ state possesses long-range charge transfer (LRCT) character.[29] D–A TADF PCs based on carbazoyl dicyanobenzenes (CDCBs) have been extensively employed in myriad photocatalytic reactions. Examples from this family of TADF PCs cover a broad range of $E_T$. For example, the $E_T$ values of **4DPAIPN**, **4CzTPN**, **2CzIPN**, **4CzIPN**, and **3,5-2CzBN** increase from 2.30 eV[30] to 2.34,[31] 2.72,[31] 2.73,[32] and 3.03 eV,[31] respectively. These values overlap with those of, for example, **[Ir(dF(CF$_3$)ppy)$_2$(dtbbpy)]PF$_6$** ($E_T$ = 2.64 eV[23]) and benzophenone ($E_T$ = 3.00 eV[33]). Beyond CDCBs, other D–A TADF PEnT PCs include **pDTCz-DPmS**[34] and **DI-PF**[35] (Fig. S2). **pDTCz-DPmS** ($E_T$ = 2.93 eV) possesses a suitable $E_T$ to photocatalyze the *E*/*Z* isomerization of diisopropyl fumarate ($E_T$ = 2.7 eV),[36] producing 81% of diisopropyl maleate while **4CzIPN** only yields 6%, owing to its lower $E_T$ of 2.68 eV.[37] **DI-PF** ($E_T$ = 2.38 eV) yielded 66% *Z*-stilbene in the *E*/*Z* isomerization of *E*-stilbene ($E_T$ = 2.2 eV) despite its lower triplet energy, while **4CzIPN** affords 87% of the desired product.[35] Another class of TADF PCs contains an imidazo-phenothiazine (IPTZ) acceptor unit connected with different donor groups. The PCs **ACR-IMAC**, **ACR-IPTZ**, and **SACR-IPTZ** have similar triplet energies of $E_T$ = 2.76 eV,[38] 2.76 eV,[39] and 2.77 eV,[39] respectively. Their use in a range of reactions, such as the [2 + 2] cycloaddition of an indole and dimethylphenylvinylsilane, afforded near quantitative product yields.[38,39] A second class of TADF compounds is the so-called multi-resonant TADF (MR-TADF) emitters. These are rigid polycyclic aromatic hydrocarbons that are typically doped with both electron-rich and electron-deficient groups. Suitable

regiochemistry of these p- and n-dopants produces an alternating pattern of increasing and decreasing electron density in the excited state as compared to the ground state, leading to the necessary small exchange energy that turns on TADF. Given the short distance between D and A motifs, the emissive excited state is of short-range CT (SRCT) character.[40] Compared to D–A TADF compounds, MR-TADF emitters have more intense low energy absorption bands, narrower emission spectra, smaller Stokes shifts, and their emission spectra show only minimal positive solvatochromism—all potentially attractive properties for their use as PCs.[40] Our group has demonstrated the broad utility of two families of MR-TADF PCs in a range of photoinduced electron transfer (PET) and PEnT reactions.[41,42] These two families contain nitrogen donor atoms and either boron or carbonyl groups as n-dopants within the polycyclic aromatic hydrocarbon framework.

We, as well as Lee and co-workers, recently showed that the acceptor moiety is not required in MR-TADF emitter design for OLEDs.[43–47] Indeed, when the nitrogen atoms in di-indolocarbazoles are *para*-disposed, there is very weak TADF as $\Delta E_{ST}$ is moderately large, resulting in slow $k_{RISC}$. **DiICztBu$_4$** and **DiICzMes$_4$** have similar $E_T$ of 2.55 (in DCM)[43] and 2.57 eV (in toluene),[44] respectively, while their reported $\Delta E_{ST}$ values are 0.29 and 0.26 eV. Recognizing their potential as PCs, herein we investigated a series of four structurally related DiICz-based TADF PCs, **DiICztBu$_4$**, **DiICzMes$_4$**, **DiICztBuCz$_4$**, and **DiICztBuDPA$_4$**, in DET reactions (Fig. 2); the first two have previously been reported, while **DiICztBuCz$_4$** and **DiICztBuDPA$_4$** were, coincident with this work, recently reported by Lee and co-workers.[48] Across the first three compounds in this series, there is a progressive stabilization of the $S_1$ state, while the $T_1$ energy is largely unaffected; both $S_1$ and $T_1$ are stabilized in **DiICztBuDPA$_4$**. Thus, the impact of $\Delta E_{ST}$ on the performance in DET is probed for the first time. While we did not observe a dependency of the efficiency of the PEnT reactions as a function of the $\Delta E_{ST}$ of the PC across five different PEnT reactions, four involving direct DET to the substrate and one nickel-sensitized dual photocatalysis reaction, we did discover that these PCs initiate fast PEnT reactions that show remarkably little sensitivity to the presence of $O_2$, despite it being a competitive triplet quencher. In the four PEnT reactions with direct energy transfer to the substrate, **DiICztBu$_4$**, **DiICzMes$_4$**, and **DiICztBuCz$_4$** consistently outperform **4CzIPN** both in terms of NMR yield and reaction rate.

## Results and discussion

The syntheses of **DiICztBu$_4$**, **DiICzMes$_4$**, **DiICztBuCz$_4$**, and **DiICztBuDPA$_4$** are detailed in the SI. The UV-vis absorption spectra of these compounds in DCM, along with that of the

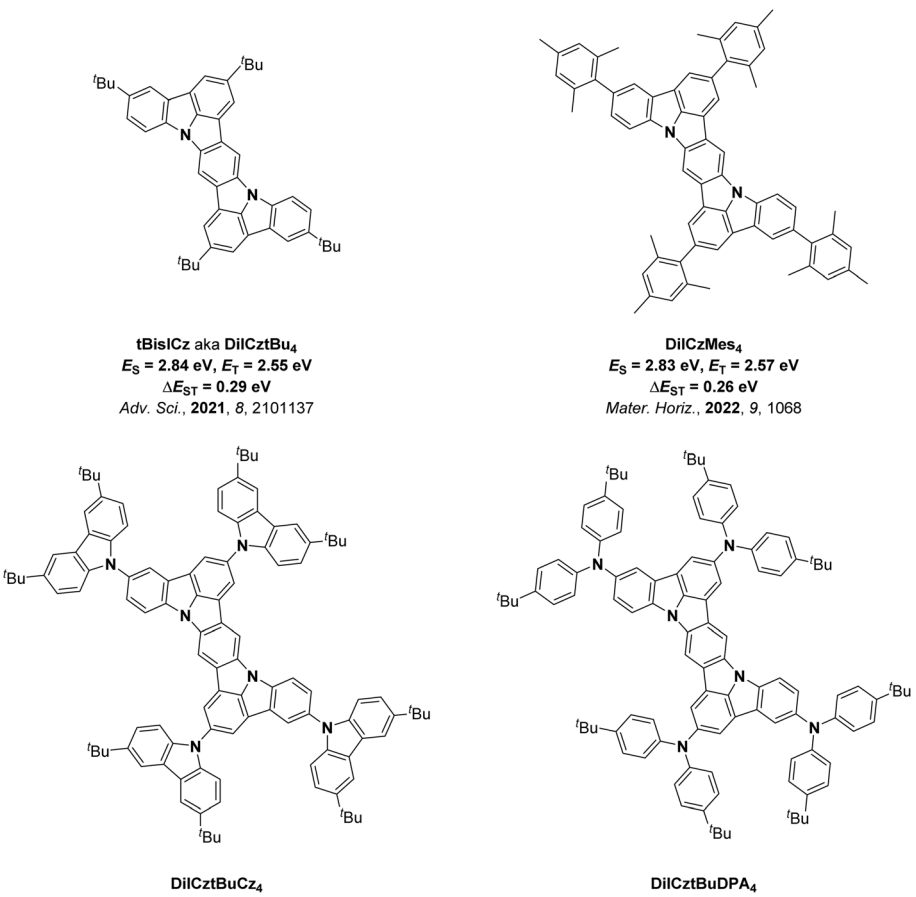


Fig. 2 Chemical structures of DiICztBu$_4$, DiICzMes$_4$, DiICztBuCz$_4$, and DiICztBuDPA$_4$.

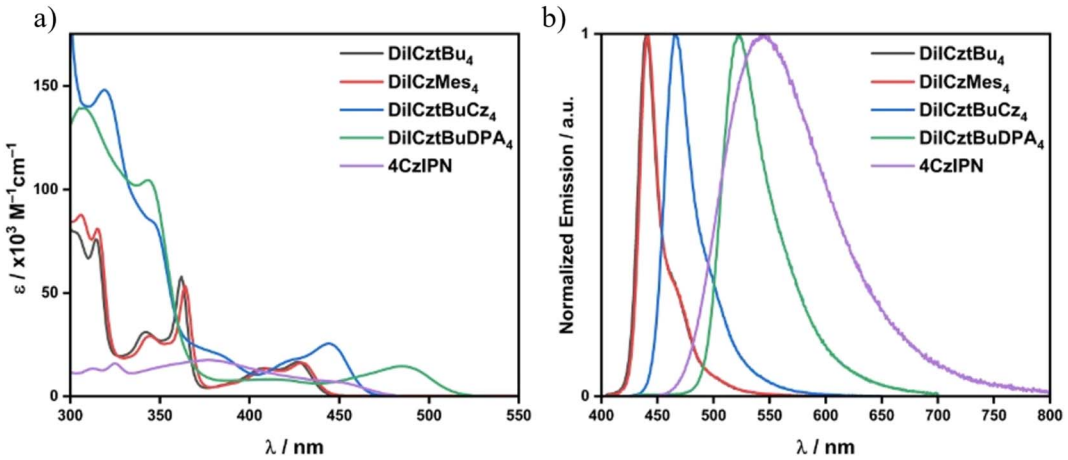


Fig. 3 (a) Absorption and (b) steady-state PL spectra in DCM of **DilCztBu$_4$** ($\lambda_{exc}$ = 340 nm), **DilCzMes$_4$** ($\lambda_{exc}$ = 380 nm), **DilCztBuCz$_4$** ($\lambda_{exc}$ = 340 nm), **DilCztBuDPA$_4$** ($\lambda_{exc}$ = 400 nm), and **4CzIPN** ($\lambda_{exc}$ = 378 nm).

reference PC **4CzIPN**, are shown in Fig. 3a. **DilCztBu$_4$**, **DilCzMes$_4$**, **DilCztBuCz$_4$**, and **DilCztBuDPA$_4$** all exhibit low-energy absorption bands in the visible region that are more intense than that of **4CzIPN**. The presence of the mesityl (Mes) groups in **DilCzMes$_4$** leads to a very slight red shift in the absorption spectrum compared to **DilCztBu$_4$**, while the substitution of the diindolocarbazole with progressively stronger carbazole (Cz) and diarylamine donors results in a larger red shift of these bands (Fig. 3a and S37). A similar trend is observed in their photoluminescence (PL) spectra (Fig. 3b), where the PL maximum in DCM shifts from $\lambda_{PL}$ of 440 to 442, 466, and 532 nm for **DilCztBu$_4$**, **DilCzMes$_4$**, **DilCztBuCz$_4$**, and **DilCztBuDPA$_4$**, respectively (Fig. 3b and Table 2). Their emission is more narrowband compared to the broad PL of **4CzIPN**, reflecting their more rigid structures.

The $S_1$ and $T_1$ energies were determined from the onsets of the steady-state PL and delayed emission (gate time: 1–9 ms) spectra in 2-MeTHF glass at 77 K, respectively (Fig. S40); the $\Delta E_{ST}$ value is the difference in energy between these two (Fig. S40 and Table 1). **DilCztBu$_4$**, **DilCzMes$_4$**, and **DilCztBuCz$_4$** have very similar $E_T$ of 2.58, 2.57, and 2.55 eV, respectively. As their emission profiles are similar, so too will be their spectral overlap with the sub, and thus the $k_{DET}$ should be comparable across these three PCs. The $S_1$ energy, $E_S$, however, progressively decreases from 2.91 to 2.84 and 2.77 eV (measured at 77 K in 2-MeTHF); thus, the $\Delta E_{ST}$ likewise narrows from 0.33 to 0.27 and 0.22 eV. The $E_S$ and $E_T$ for **DilCztBuDPA$_4$** are 2.54 and 2.41 eV, resulting in the smallest $\Delta E_{ST}$ of 0.13 eV. The $E_T$ values determined at cryogenic temperatures of these four derivatives are all lower than the 2.73 eV of **4CzIPN** (Fig. S40e). **DilCztBu$_4$** and **DilCzMes$_4$** have previously been reported as MR-TADF emitters, and given the similar photophysical properties of **DilCztBuCz$_4$** and **DilCztBuDPA$_4$** to these two, the high molar absorptivity of the low-energy absorption band, the minimal positive PL solvatochromism, the narrowband emission and the small $\Delta E_{ST}$, they can also be classified as MR-TADF (Table 2).

While the low temperature (LT) measurements, at 77 K, permit a robust estimation of $\Delta E_{ST}$, noting that in the vast majority of TADF compounds the $S_1$ state has greater CT character than $T_1$, this measurement will not accurately capture $E_S$ at room temperature (RT) in solution. This is because CT states are stabilized as a function of solvent polarity, and the greater the CT character, the stronger the stabilization of the state.[50] As triplet states tend to show lesser CT character than singlets, the estimated $E_T = E_S(RT) - \Delta E_{ST}(LT)$ represents the outer bound value for what $E_T$ may be at room temperature. Thus, given the LRCT character of the $S_1$ state of **4CzIPN**, the change in $E_T$ at room temperature is more pronounced than for the four DiICz MR-TADF compounds (Table 1). This implies that in DET reactions, the spectral overlap between the PC* and the sub may change significantly, especially when the $T_1$ state possesses some CT character. For MR-TADF compounds, this stabilization effect is small given the SRCT character of the $S_1$ and $T_1$ states. So, at low temperature, the $E_T$ values are 2.58, 2.57, 2.55, and 2.41 eV in 2-MeTHF for **DilCztBu$_4$**, **DilCzMes$_4$**, **DilCztBuCz$_4$**, and **DilCztBuDPA$_4$**, respectively, while in DCM at room

Table 1 Excited-state energies for DilCztBu$_4$, DilCzMes$_4$, DilCztBuCz$_4$, DilCztBuDPA$_4$, and 4CzIPN

| | 77 K values[a] | | | Room temperature $E_T$[b]/eV | | | |
|---|---|---|---|---|---|---|---|
| Compound | $E_S$/eV | $E_T$/eV | $\Delta E_{ST}$/eV | Toluene | EtOAc | DCM | DMF |
| **DilCztBu$_4$** | 2.91 | 2.58 | 0.33 | 2.60 | 2.63 | 2.60 | 2.61 |
| **DilCzMes$_4$** | 2.84 | 2.57 | 0.27 | 2.64 | 2.66 | 2.65 | 2.65 |
| **DilCztBuCz$_4$** | 2.77 | 2.55 | 0.22 | 2.58 | 2.61 | 2.58 | 2.58 |
| **DilCztBuDPA$_4$** | 2.54 | 2.41 | 0.13 | 2.44 | 2.45 | 2.40 | 2.46 |
| **4CzIPN** | 2.77 | 2.73 | 0.04 | 2.67 | 2.66 | 2.56 | 2.54 |

[a] 77 K values were measured in 2-MeTHF glass. $E_S$ was determined from the onset of the steady-state PL and $E_T$ from the onset of the gated emission acquired in a time window of 1–9 ms after excitation. $\Delta E_{ST} = E_S - E_T$. $\lambda_{exc}$ = 390 nm for **DilCztBu$_4$**, **DilCzMes$_4$**, and **DilCztBuCz**; $\lambda_{exc}$ = 400 nm for **DilCztBuDPA$_4$** and $\lambda_{exc}$ = 380 nm for **4CzIPN**. [b] Room temperature $E_T$ values were estimated following our previously reported methodology,[49] where $E_T(RT) = E_S(RT) - \Delta E_{ST}(LT)$, with $E_S(RT)$ being the onset of the steady-state PL in the respective solvents and $\Delta E_{ST}(LT)$ being measured in 2-MeTHF at 77 K.

Table 2 Solution-state photophysical properties of **DiICztBu$_4$**, **DiICzMes$_4$**, **DiICztBuCz$_4$**, and **DiICztBuDPA$_4$** and the reference photocatalysts 4CzIPN and *fac*-Ir(ppy)$_3$

| Compound | $\lambda_{abs}$[a]/nm ($\varepsilon$/10$^3$ M$^{-1}$ cm$^{-1}$) | $\lambda_{PL}$[a]/nm | $E_S$[b]/eV | $E_T$[b]/eV | $\Delta E_{ST}$ | $\tau_{PL}$[c]/ns |
|---|---|---|---|---|---|---|
| **DiICztBu$_4$** | 305 (58), 315 (67), 343 (29), 362 (54), 408 (13), 427 (16) | 440 | 2.91 | 2.58 | 0.33 | 9 (8) |
| **DiICzMes$_4$** | 300 (84), 306 (88), 315 (81), 344 (29), 364 (53), 409 (13), 430 (16) | 442 | 2.84 | 2.57 | 0.27 | 10 (8) |
| **DiICztBuCz$_4$** | 319 (152), 347 s (84), 385 s (20), 420 s (17), 444 (25) | 466 | 2.77 | 2.55 | 0.22 | 10 (8) |
| **DiICztBuDPA$_4$** | 305 (141), 343 (104), 411 (7), 485 (14) | 523 | 2.54 | 2.41 | 0.13 | 16 (13) |
| **4CzIPN** | 313 (14), 325 (16), 377 (18), 450 s (7) | 544 | 2.77 | 2.73 | 0.04 | 1896 (218)[d] |
| ***fac*-Ir(ppy)$_3$** | 344 (10), 378 (13), 409 (8), 455 (3) | 520 | — | 2.58 | — | 1391 (54) |

[a] In DCM at 77 K, taken from the onset of steady-state PL spectrum for $E_S$ and the onset of the gated emission spectrum (1–9 ms) for $E_T$. [b] In 2-MeTHF at 77 K, taken from the onset of steady-state PL spectrum for $E_S$ and the onset of the gated emission spectrum (1–9 ms) for $E_T$. [c] Under degassed conditions, excited-state lifetimes in air in parentheses. [d] Lifetime is the average lifetime of **4CzIPN** calculated as $\tau_{avg} = \tau_1 \times w_1 + \tau_2 \times w_2$.

temperature, the $E_T$ values remain essentially the same at 2.60, 2.65, 2.58, and 2.40 eV, respectively (Table 1). This contrasts with the effect on the $T_1$ energy of **4CzIPN** ($E_T$(LT) = 2.73 eV *vs.* $E_T$(RT) = 2.56 eV; where LT is low temperature, 77 K, and RT is room temperature). This is illustrated in a comparison between the $T_1$ energies in 2-MeTHF glass and DCM solutions, $\Delta E_{T-T}$, which is 0.08 eV for **DiICzMes$_4$** and 0.17 eV for **4CzIPN**. Thus, these four MR-TADF compounds maintain their $E_T$ in polar solvents, while for **4CzIPN**, the $E_T$ is much more stabilized. The time-resolved PL decays of **DiICztBu$_4$**, **DiICzMes$_4$**, **DiICztBuCz$_4$**, and **DiICztBuDPA$_4$** in DCM are shown in Fig. S40 and S41 and are listed in Table 2. There is no delayed emission, and PL lifetimes range from 9–16 ns. Given the moderately large $\Delta E_{ST}$, it is not uncommon for MR-TADF emitters to not show delayed emission in solution as non-radiative decay competes with RISC, while in the solid state, this is largely suppressed, and delayed emission becomes apparent.

## DET reactions

We began by studying intramolecular DET reactions with photocatalysts of increasing triplet energy to focus on the interaction between the PC and a single molecule. We first investigated the *E*/*Z* isomerization of an alkene, *E*-cinnamyl acetate, with a $T_1$ energy similar to those of the MR-TADF emitters; notably, the structurally similar *E*-methyl cinnamate has a $E_T$ = 2.38 eV [51] (Table S7). We expect the triplet energy of *E*-cinnamyl acetate, which contains a methylene group between the styrenyl moiety and the ester group, to be slightly higher compared to *E*-methyl cinnamate, which has a larger conjugation length. The geometric isomerization does not take place in the absence of an irradiated PC (Table 3, entries 1 and 2). After 24 h of irradiation under $N_2$, the use of **DiICztBu$_4$**, **DiICzMes$_4$**, and **DiICztBuCz$_4$** as PCs yielded comparable *E*/*Z* ratios of 18/82, 19/81, and 19/81, respectively (Table 3, entries 4, 6, and 8), performing as well in this reaction as **4CzIPN** (*E*/*Z* ratio of 14/86, Table 3, entry 12). Similar *E*/*Z* ratios are observed under air (*E*/*Z* = 19/81, 17/84, 20/80, and 15/85 for **DiICztBu$_4$**, **DiICzMes$_4$**, **DiICztBuCz$_4$**, and **4CzIPN**, respectively, Table 3, entries 3, 5, 7, and 11). Amazingly, the end ratio obtained for this DET reaction is unaffected despite $O_2$ being a competitive triplet quencher. This is, however, not the case with **DiICztBuDPA$_4$**, which under $N_2$ yielded an *E*/*Z* ratio of 28/72, a lower ratio than those obtained with the other PCs, while there is effectively no isomerization observed in air (Table 3, entries 9 and 10).

Fig. 4 shows the reaction progression for the *E*/*Z* isomerization of cinnamyl acetate in air at short times, while for **DiICztBuDPA$_4$**, the reaction under $N_2$ is shown. The conversion saturates after 30 min for **DiICztBu$_4$**, **DiICzMes$_4$**, and **DiICztBuCz$_4$**, with these PCs having similar reaction rates. There is no correlation observed between $\Delta E_{ST}$ and either the *E*/*Z* ratio or reaction rate for this transformation. The absence of any substantive change in the post-reaction absorption spectra of **DiICztBu$_4$**, **DiICzMes$_4$**, and **DiICztBuCz$_4$** revealed that these compounds are photochemically stable to $O_2$ under the reaction conditions (Fig. S46a–c). Given that $O_2$ does not affect the *E*/*Z*

Table 3 *E*/*Z* isomerization of cinnamyl acetate[a]

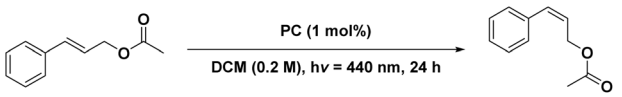


| Entry | Photocatalyst | Conditions | *E*/*Z* ratio |
|---|---|---|---|
| 1 | None | Air | 99/1 ± 0 |
| 2 | None | $N_2$ | 99/1 ± 0 |
| 3 | **DiICztBu$_4$** | Air | 19/81 ± 0 |
| 4 | **DiICztBu$_4$** | $N_2$ | 18/82 ± 0 |
| 5 | **DiICzMes$_4$** | Air | 16/84 ± 1 |
| 6 | **DiICzMes$_4$** | $N_2$ | 19/81 ± 0 |
| 7 | **DiICztBuCz$_4$** | Air | 20/80 ± 0 |
| 8 | **DiICztBuCz$_4$** | $N_2$ | 19/81 ± 0 |
| 9 | **DiICztBuDPA$_4$** | Air | 98/2 ± 0 |
| 10 | **DiICztBuDPA$_4$** | $N_2$ | 28/72 ± 0 |
| 11 | **4CzIPN** | Air | 15/85 ± 0 |
| 12 | **4CzIPN** | $N_2$ | 14/86 ± 0 |

[a] Cinnamyl acetate (0.2 mmol) in DCM (0.2 M) with 1 mol% PC loading. *E*/*Z* ratios were determined *via* $^1$H NMR spectroscopy. Reported yields are the mean from at least two reactions with associated standard deviations.

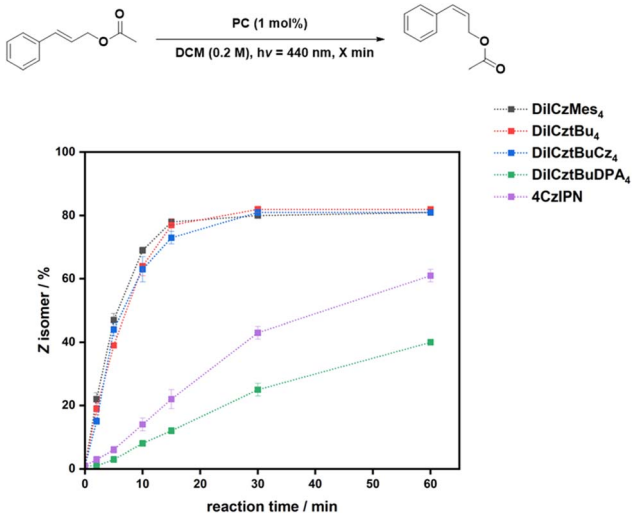


Fig. 4 Reaction progression for the *E*/*Z* isomerization of cinnamyl acetate in air unless otherwise noted. *E*/*Z* ratios are given in % *Z* isomer after *x* minutes ($\lambda_{exc}$ = 440 nm). Cinnamyl acetate (0.2 mmol) in DCM (0.2 M) and PC (1 mol%). *E*/*Z* ratios were determined by $^1$H NMR spectroscopy. Reactions with **DilCztBuDPA$_4$** as the PC were performed under $N_2$.

ratio, we investigated the effect on the reaction kinetics as a function of the presence/absence of $O_2$ by comparing the *E*/*Z* ratios after 5 min. The reaction rates slightly increase in the absence of $O_2$, leading to slightly improved *E*/*Z* ratios of 48/52, 51/49, and 49/51 for **DilCztBu$_4$**, **DilCzMes$_4$**, and **DilCztBuCz$_4$**, respectively, from those in air (53/47, 61/39, and 56/44, respectively); it is not clear why the change is more dramatic with **DilCzMes$_4$**. Hence, $O_2$ acts as an ineffective yet competitive quencher of the triplet excited state of these PCs, as the change in the *E*/*Z* ratio at early times is marginal. The contrasting results with **DilCztBuDPA$_4$** are discussed in the SI.

The isomerization reaction with **4CzIPN** is significantly slower than with **DilCztBu$_4$**, **DilCzMes$_4$**, and **DilCztBuCz$_4$**, only producing a 39/61 *E*/*Z* ratio after 60 min (Fig. 4). Thus, despite similar thermodynamic driving forces (*i.e.*, similar $E_T$), the origin of the higher yields of the *Z* isomer and faster reaction kinetics could be due to either the higher molar absorptivity of these three MR-TADF compounds at the photoexcitation wavelength and/or an increased spectral overlap of the phosphorescence of the MR-TADF emitters with the spin-forbidden absorption of the sub. **4CzIPN** is mostly photostable; however, a slight decrease in the absorbance of the CT band is observed in air, suggesting that some degradation is taking place if the reaction is carried out when $O_2$ is present (Fig. S46e). Furthermore, there is a significant dependency of the kinetics of the reaction with respect to the presence/absence of $O_2$. After 5 min, the *E*/*Z* ratios are 80/20 and 94/6 under $N_2$ and air, respectively. These results reveal that **4CzIPN** photocatalyzes this reaction much more slowly than **DilCztBu$_4$**, **DilCzMes$_4$**, and **DilCztBuCz$_4$** and that its triplet excited state is also more strongly quenched by $O_2$. The excited-state lifetimes of the PCs under aerated conditions are 8, 8, 8, and 13 ns for **DilCztBu$_4$**, **DilCzMes$_4$**, **DilCztBuCz$_4$**, and **DilCztBuDPA$_4$**, respectively. These are not affected by the presence of *E*-cinnamyl acetate ($\tau_{PL}$ of 8, 8, 8, and 12 ns for **DilCztBu$_4$**, **DilCzMes$_4$**, **DilCztBuCz$_4$**, and **DilCztBuDPA$_4$**, respectively, Fig. S47).

We had previously assessed MR-TADF compounds **DABNA-1**, ***t*DABNA**, **CzBN**, and **DtBuCzB** as photocatalysts in the *E*/*Z* isomerization of cinnamyl acetate. Of these, **CzBN** produced the highest conversion to the *Z* isomer in a ratio of 19/81 after two hours in air (in THF); the ratio remained the same after 24 hours.[42] In our previous study, we did not monitor the reaction kinetics at shorter times. Thus, **CzBN** yields a similar *E*/*Z* ratio as the DiICz photocatalysts (19/81 for **CzBN** after 2 h and 18/82 for **DilCztBu$_4$** after 1 h). This is consistent with their comparable $E_T$ values (2.58 eV for **CzBN** and 2.58 eV for **DilCztBu$_4$**, respectively, in 2-MeTHF at 77 K).[42]

We next investigated the *E*/*Z* isomerization of diisopropyl fumarate, which has a higher $E_T$ of 2.7 eV,[31] to produce the corresponding maleate ($E_T$ = 3.1 eV)[31] (Table S8). Despite the $E_T$s of the PCs being lower than 2.7 eV (Table 2), both **DilCztBu$_4$** ($E_T$ = 2.60 in DCM) and **DilCzMes$_4$** ($E_T$ = 2.65 in DCM) photocatalyzed the reaction, producing identical *E*/*Z* ratios of 13/87 after 24 h (Table 4, entries 4 and 6). **DilCztBuCz$_4$** and **4CzIPN** were less effective, producing *E*/*Z* ratios of 66/34 and 69/31, respectively (Table 4, entries 8 and 12). Surprisingly, it seems that the slightly lower $E_T$ of **DilCztBuCz$_4$** (2.58 eV in DCM) compared to **DilCzMes$_4$** ($E_T$ = 2.65 eV in DCM) and **DilCztBu$_4$** ($E_T$ = 2.60 eV in DCM) is responsible for these large changes in *E*/*Z* ratios; notably, **DilCztBuCz$_4$** is unstable under the reaction conditions (Fig. S46c). These results also clearly illustrate the effect of solvent polarity on the magnitude of the spectral overlap between the PC and sub, and the corresponding efficiency to photocatalyze the isomerization. Despite **4CzIPN** having the highest $E_T$ of 2.73 eV in 2-MeTHF at 77 K, meaning that if these values were reflective of accessible triplet energies

Table 4 *E*/*Z* isomerization of diisopropyl fumarate[a]

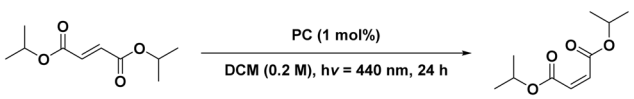


| Entry | Photocatalyst | Conditions | *E*/*Z* ratio |
|---|---|---|---|
| 1 | None | Air | 100/0 ± 0 |
| 2 | None | $N_2$ | 100/0 ± 0 |
| 3 | **DilCztBu$_4$** | Air | 95/5 ± 1 |
| 4 | **DilCztBu$_4$** | $N_2$ | 13/87 ± 0 |
| 5 | **DilCzMes$_4$** | Air | 92/8 ± 2 |
| 6 | **DilCzMes$_4$** | $N_2$ | 13/87 ± 0 |
| 7 | **DilCztBuCz$_4$** | Air | 88/12 ± 0 |
| 8 | **DilCztBuCz$_4$** | $N_2$ | 66/34 ± 4 |
| 9 | **DilCztBuDPA$_4$** | Air | 100/0 ± 0 |
| 10 | **DilCztBuDPA$_4$** | $N_2$ | 100/0 ± 0 |
| 11 | **4CzIPN** | Air | 91/9 ± 4 |
| 12 | **4CzIPN** | $N_2$ | 69/31 ± 4 |

[a] Diisopropyl fumarate (0.2 mmol) in DCM (0.2 M) with 1 mol% PC loading. *E*/*Z* ratios were determined by $^1$H NMR spectroscopy. Reported yields are the mean from at least two reactions with associated standard deviations.

under the reaction conditions, then it should be able to photocatalyze the isomerization to a similar extent as the DiICz PCs. The triplet state of **4CzIPN**, however, shows the greatest stabilization as a function of solvent polarity ($E_T$ in DCM is 2.56 eV at room temperature, Table 1). This accounts for the poorer *E*/*Z* ratio of 69/31 (Table 4, entry 12). Notably, as **4CzIPN** is photostable under these reaction conditions when performed under $N_2$, its poor performance cannot be attributed to PC degradation (Fig. S45e).

In contrast to cinnamyl acetate (Table 3), the *E*/*Z* isomerization of diisopropyl fumarate essentially does not proceed to any appreciable extent in the presence of $O_2$, with *E*/*Z* ratios of 96/5, 93/8, 88/12, and 91/9 for **DiICztBu$_4$**, **DiICzMes$_4$**, **DiICztBuCz$_4$**, and **4CzIPN**, respectively (Table 4, entries 3, 5, 7, and 11). **DiICztBuDPA$_4$** could not photocatalyze the reaction (Table 4, entries 9 and 10), given its $E_T$ of 2.41 eV.

To understand the divergence in the behavior of these two isomerization reactions in the presence of $O_2$, we interrogated the reaction rates of diisopropyl fumarate under $N_2$ (Fig. 5). If the rates are slower compared to those with cinnamyl acetate, then the lower *E*/*Z* ratios may be explained by competitive $O_2$ quenching of the $T_1$ state to that of the fumarate. Unlike the reaction with cinnamyl acetate, the reaction rates under $N_2$ differ between **DiICzMes$_4$**, **DiICztBu$_4$**, and **DiICztBuCz$_4$**, but still are all faster than **4CzIPN**. The fastest conversion to the *Z* isomer uses **DiICzMes$_4$**, yielding an *E*/*Z* ratio of 22/79 ± 3 after 60 min (13 : 87 after 24 h, Table 4, entry 6), while **DiICztBu$_4$** only produces an *E*/*Z* ratio of 60/41 ± 1 after 60 min, yet affords the same *E*/*Z* ratio after 24 h as **DiICzMes$_4$** (13 : 87 after 24 h, Table 4, entry 4). The reaction reaches its steady-state *E*/*Z* ratio after 2 h for **DiICzMes$_4$** (*E*/*Z* ratio of 12/88), while for **DiICztBu$_4$** it takes 4 h to reach the 13/87 *E*/*Z* ratio. These rates are slower than those with cinnamyl acetate, where the reaction was completed after 30 min. Given that both **DiICzMes$_4$** and **DiICztBu$_4$** are stable during the reaction when conducted under $N_2$, photodegradation of the PC can be excluded as the origin of the slower reaction kinetics observed for **DiICztBu$_4$**. As the phosphorescence of both **DiICztBu$_4$** and **DiICzMes$_4$** is the same, the spectral overlap between the phosphorescence spectra of these two PCs and the spin-forbidden absorption spectrum of the sub will therefore be similar. A plausible conclusion is that the *tert*-butyl groups are bulkier than mesityl groups and impede the collisional interaction more, thus adversely affecting the reaction kinetics with **DiICztBu$_4$**. We observed that these two PCs do photodegrade when the reaction is carried out under air. Thus, there is a divergence in the photochemical outcome wherein the kinetics of the *E*/*Z* isomerization of cinnamyl acetate outcompetes photodegradation, while this is not the case with the *E*/*Z* isomerization of diisopropyl fumarate (Fig. S45a and b). Surprisingly, while the initial rate of isomerization using **DiICztBuCz$_4$** is comparatively as fast as using **DiICzMes$_4$**, there is a significant off-cycle photodegradation both in air and $N_2$ that effectively caps the *E*/*Z* ratio at only 66/34 ± 4 (Fig. S45c). **DiICztBuDPA$_4$** is photostable when the reaction is conducted under $N_2$, while there are changes in the absorption spectrum when the reaction is conducted in air (Fig. S46d). Hence, the fact that the reaction does not proceed is a consequence of there being no spectral overlap between the phosphorescence of **DiICztBuDPA$_4$** and the spin-forbidden absorption of the substrate.

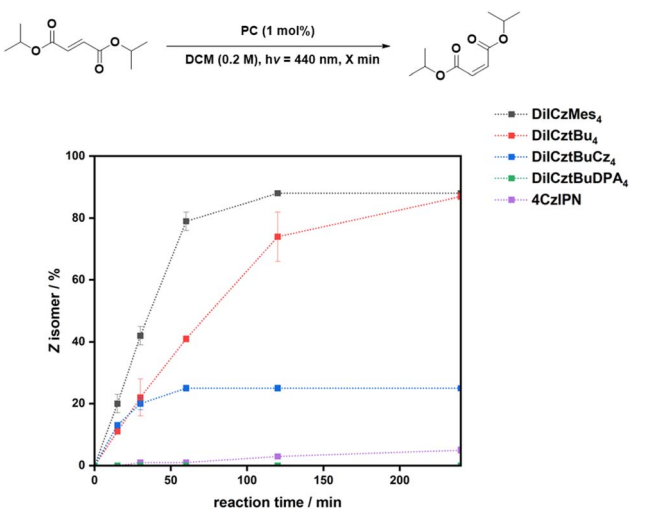


Fig. 5 Reaction progression for the *E*/*Z* isomerization of diisopropyl fumarate under $N_2$. *E*/*Z* ratios are given in % *Z* isomer after *x* minutes irradiated at 440 nm. Diisopropyl fumarate (0.2 mmol) in DCM (0.2 M) and PC (1 mol%). *E*/*Z* ratios were determined by $^1$H NMR spectroscopy.

**4CzIPN** is significantly slower and less efficient in this isomerization reaction, producing a steady-state *E*/*Z* ratio of only 69/31 ± 4 after 24 h (Table 4, entry 12); indeed, after 4 h, there is only an *E*/*Z* ratio of 95/5 ± 1 (Table S8). Under these conditions, **4CzIPN** is photostable under $N_2$; however, in air, photodegradation of **4CzIPN** is observed (Fig. S46e). Thus, the poor performance of **4CzIPN** can be explained by the too-small spectral overlap with the fumarate substrate.

The *E*/*Z* isomerization of diisopropyl fumarate studies demonstrate that three of these PCs can catalyze PEnT reactions with substrates having $E_T$ of 2.7 eV.[31] Thus, we next explored the intramolecular [2 + 2] cycloaddition of norbornadiene ($E_T$ = 2.7 eV [52]) to quadricyclane (Table S9). Schmid *et al.* had reported a 99% yield after one hour using an anionic Ir complex having an $E_T$ of 2.99 eV (Table 5, entry 14).

The reaction does not take place in the absence of a PC (Table 5, entries 1 and 2). After 30 min reaction time using **DiICztBu$_4$**, quadricyclane was obtained in an 89% yield under $N_2$ (Table 5, entry 5). In contrast to the *E*/*Z* isomerization of fumarate, **DiICzMes$_4$** and **DiICztBuCz$_4$** perform as well as **DiICztBu$_4$**, yielding 85, 88, and 89%, respectively, after 30 min (Table 5, entries 5, 7, and 9). The reaction is slightly quenched in the presence of $O_2$, producing yields of 64, 71, and 75% after 30 min when using **DiICztBu$_4$**, **DiICzMes$_4$**, and **DiICztBuCz$_4$**, respectively (Table 5, entries 3, 6, and 8). Given the fast reaction rates, there is thus significantly less quenching of the $^3$PC* by $O_2$ than what has been observed with diisopropyl fumarate. Again, it is not surprising that **DiICztBuDPA$_4$** does not photocatalyze the reaction, given its too low $E_T$ (Table 5, entries 10 and 11). Similarly, given that **4CzIPN** did not photoisomerize diisopropyl fumarate to diisopropyl maleate after 30 min to any appreciable extent, this PC did not photocatalyze the [2 + 2]

Table 5 [2 + 2] cycloaddition of norbornadiene[a]

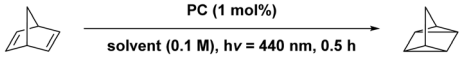


| Entry | Photocatalyst | Conditions | Yield/% |
|---|---|---|---|
| 1 | None | Air | 0 ± 0 |
| 2 | None | $N_2$ | 0 ± 0 |
| 3 | **DiICztBu$_4$** | Air | 64 ± 4 |
| 4 | **DiICztBu$_4$** | $N_2$, 2 h | 87 ± 1 |
| 5 | **DiICztBu$_4$** | $N_2$ | 89 ± 2 |
| 6 | **DiICzMes$_4$** | Air | 71 ± 6 |
| 7 | **DiICzMes$_4$** | $N_2$ | 85 ± 5 |
| 8 | **DiICztBuCz$_4$** | Air | 75 ± 2 |
| 9 | **DiICztBuCz$_4$** | $N_2$ | 88 ± 0 |
| 10 | **DiICztBuDPA$_4$** | Air | 0 ± 0 |
| 11 | **DiICztBuDPA$_4$** | $N_2$ | 0 ± 0 |
| 12 | **4CzIPN** | Air | 0 ± 0 |
| 13 | **4CzIPN** | $N_2$ | 0 ± 0 |
| 14 | $[Ir(L)_2(BCF)_2]^-$ | Degassed | 99[b] |

[a] Norbornadiene (0.2 mmol) and PC (1 mol%) in DCM (2 mL). Yields were determined by $^1$H NMR spectroscopy using 1,3,5-trimethoxybenzene as the internal standard. [b] From ref. 52 in $CD_3CN$, $\lambda_{exc}$ = 415 nm after 1 h, norbornadiene (0.05 mmol), PC (0.3 mol%), $CD_3CN$ (0.6 mL). Reported yields are the mean from at least two reactions with associated standard deviations.

cycloaddition of norbornadiene within 30 min (Table 5, entries 12 and 13). These results not only demonstrate the value of three of these MR-TADF PCs to photocatalyze a demanding PEnT reaction but also that $E_T$ as a parameter is too coarse when cross-comparing different reactions using substrates with similar $E_T$. We had previously demonstrated that **DiKTa**, another MR-TADF photocatalyst ($E_T$ = 2.62 eV),[41] could efficiently photoisomerize diisopropyl fumarate into diisopropyl maleate in a ratio of 10/90 in MeCN over 16 h, a similar ratio to that using **DiICzMes$_4$** (8/92); in this earlier study, the reaction progression at shorter reaction times was not analysed.[41]

The photostability of the PCs was tested under the reaction conditions under $N_2$ and in air (Fig. S51). The absorption spectra of **DiICztBu$_4$**, **DiICzMes$_4$**, and **DiICztBuCz$_4$** show only a minimal decrease in intensity under $N_2$, while there are greater changes with $O_2$ present that suggest more photodegradation, which is consistent with the less efficient performance when the reaction is carried out in air (Fig. S51a–c). Interestingly, the small degree of photodegradation of the MR-TADF PCs in the [2 + 2] cycloaddition in air contrasts with the significant photodegradation in the *E*/*Z* isomerization with diisopropyl fumarate in air and the associated absence of product formation, despite both substrates having the same reported $E_T$.

There is significant photodegradation observed for **4CzIPN** under $N_2$, and the profile is similar to that in air (Fig. S51e). The absorption band at $\lambda_{abs}$ = 377 nm and the shoulder at $\lambda_{abs}$ = 450 nm disappear, while a more red-shifted, less intense band at $\lambda_{abs}$ = 520 nm appears. These results imply that the substrate reacts with **4CzIPN** and that the [2 + 2] cycloaddition is likely a radical stepwise process as opposed to a concerted mechanism (Table 5, entry 12 and 13).

We then explored a PEnT reaction with a substrate having a higher $E_T$, the sigmatropic shift of (*S*)-verbenone ($E_T$ = 3.0 eV)[52] to chrysanthenone (Table S10). This rearrangement has been used in the synthesis of the natural product xishacorene B, where verbenone was directly irradiated in the first step with UV light ($\lambda_{exc}$ = 365 nm), yielding 67% chrysanthenone.[53] Schmid *et al.* showed that this transformation can be photocatalyzed using the same iridium isocyanoborato complex as was used in the [2 + 2] cycloaddition of norbornadiene,[52] whereupon irradiating the solution at 415 nm produced the desired product in 80% yield after 180 min (Table 6, entry 10). With **DiICztBu$_4$**, **DiICzMes$_4$**, and **DiICztBuCz$_4$** as the PCs, the yields were generally low after 24 h at 29, 22, and 18%, respectively, using 1 mol% PC (Table 6, entries 2, 4, and 6); evidently, **DiICztBuDPA$_4$** cannot photocatalyze this reaction due to its too low $E_T$ (Table 6, entry 8). The yields were improved by increasing the PC loading to 5 mol%, resulting in yields of 37, 38, and 21% for **DiICztBu$_4$**, **DiICzMes$_4$**, and **DiICztBuCz$_4$**, respectively (Table 6, entries 3, 5, and 7). Using **4CzIPN** afforded only 5% product yield at 5 mol% PC loading (Table 6, entry 9).

There is essentially no change in the absorption profiles of **DiICztBu$_4$**, **DiICzMes$_4$**, and **DiICztBuCz$_4$** before and after irradiation, suggesting that any photodegradation of the PCs is not the cause for the low yields in this reaction but rather the too low triplet energy (Fig. S53a–c). **4CzIPN** and **DiICztBuDPA$_4$** are stable under the reaction conditions (Fig. S53d and e), and the 5% yield for **4CzIPN** and the 0% yield for **DiICztBuDPA$_4$** can be attributed to each having a $T_1$ energy that is effectively too low to enable DET with any degree of efficiency.

Thus far, we have explored four intramolecular PEnT reactions. To expand the portfolio of available reactions, we next investigated an example of a bimolecular cross-coupling reaction. This is frequently achieved by combining the photocatalytic cycle with a Ni-mediated cross-coupling reaction. In

Table 6 Sigmatropic shift of (*S*)-verbenone[a]

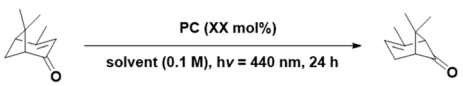


| Entry | PC | Loading/mol% | Yield/% |
|---|---|---|---|
| 1 | None | — | 0 ± 0 |
| 2 | **DiICztBu$_4$** | 1 | 29 ± 3 |
| 3 | **DiICztBu$_4$** | 5 | 37 ± 1 |
| 4 | **DiICzMes$_4$** | 1 | 22 ± 2 |
| 5 | **DiICzMes$_4$** | 5 | 38 ± 6 |
| 6 | **DiICztBuCz$_4$** | 1 | 18 ± 1 |
| 7 | **DiICztBuCz$_4$** | 5 | 21 ± 2 |
| 8 | **DiICztBuDPA$_4$** | 1 | 0 ± 0 |
| 9 | **4CzIPN** | 5 | 5 ± 1 |
| 10 | $[Ir(L)_2(BCF)_2]^-$ | 0.3 | 80[b] |

[a] (*S*)-verbenone (0.2 mmol) in DCM (0.1 M) with given PC loadings. Yields were determined by $^1$H NMR spectroscopy using 1,3,5-trimethoxybenzene as the internal standard. [b] From ref. 52 in $CD_3CN$ with $h\nu$ = 415 nm after 3 h. Reported yields are the mean from at least two reactions with associated standard deviations.

such dual-catalyzed reactions, the PC can either be involved in a PET mechanism, a so-called metallaphotoredox reaction, or in a PEnT reaction to sensitize the Ni co-catalyst by DET after it has undergone oxidative addition and transmetallation steps. This photoactivation accelerates the reductive elimination of the product.[31] One such cross-coupling reaction where the PC is purported to engage in DET is an esterification involving aryl halides being cross-coupled with carboxylic acids, where Welin *et al.* used ***fac*-Ir(ppy)$_3$** as the PC ($E_T$(***fac*-Ir(ppy)$_3$) = 2.58 eV).[13] In this cross-coupling reaction, an undesired side product is lactone **2** (Table 7). Several groups have employed organic PCs such as **4DPAPN** or **SACR-IPTZ** for these reactions (Fig. S1).[31,39] **4DPAPN**, after optimization of the reaction conditions, yielded 91% of 4-(trifluoromethyl)phenyl benzoate in the cross-coupling of benzoic acid with 4-bromobenzotrifluoride as substrates.[31] With the same substrates but under slightly different conditions, Welin *et al.* reported an 86% yield using ***fac*-Ir(ppy)$_3$** as the PC. The reaction photocatalyzed using **SACR-IPTZ** yielded 99% of the coupled product between 5-bromophthalide and benzoic acid, and no protodehalogenated product was observed.[39]

We first investigated the use of different Ni precursors in the presence of dtbbpy as an ancillary ligand under conditions similar to those reported by Hojo *et al.*[39] We changed the solvent from DMF to DCM, as the DiICz PCs are more soluble in the latter.[39] We observe a generally higher product yield in DCM when using Ni(COD)$_2$ than with NiBr$_2$·glyme, regardless of the choice of PC. The use of **DiICzMes$_4$** yielded 65% in combination with Ni(COD)$_2$, while using NiBr$_2$·glyme only results in a 41% yield (Table 7, entries 5 and 6). In both cases, side product **2** is observed in 30 and 19% yield (Table 7, entries 5 and 6). **DiICztBu$_4$**, **DiICzMes$_4$**, and **DiICztBuCz$_4$** perform similarly in combination with Ni(COD)$_2$ with yields of 59, 65, and 60% of **1**, respectively, while **2** formed in 28, 28, and 31% yield, respectively (Table 7, entries 3, 5, and 8). Changing the Ni source to NiBr$_2$·glyme yielded 31/15 and 41/19% of **1** and **2** using **DiICztBu$_4$** and **DiICzMes$_4$**, respectively, implying that the use of NiBr$_2$·glyme results in more undesired protodehalogenated product for these two complexes, while with **DiICztBuCz$_4$**, the reaction proceeds less readily, affording 20% of each of **1** and **2**. These PCs produce higher yields of **1** in combination with Ni(COD)$_2$ than using **4CzIPN** (43%, Table 7, entry 12), and this is correlated to a greater amount of **2** forming (36%) with this latter PC. When ***fac*-Ir(ppy)$_3$** is employed as the PC in combination with Ni(COD)$_2$, 65% of **1** and 15% of **2** form (Table 7, entry 14). A comparable yield is observed with **DiICzMes$_4$** (68/18% of **1** and **2**, Table 7, entry 7), but the Ni source must be [Ni(dtbbpy)(OH$_2$)$_4$]Cl$_2$, implying that the kinetics of the formation of the active Ni species are suboptimally aligned with the kinetics of DET with this PC. After solvent optimization with the best performing DiICz PC, **DiICzMes$_4$**, the coupled product **1** was obtained in a 74% yield when using a 1 : 1 mixture of DMSO : toluene (Table 8, entry 4), while the control experiment with ***fac*-Ir(ppy)$_3$** yielded a comparable yield of 77% (Table 8, entry 6). The 1 : 1 DMSO : toluene solvent system had previously been shown to be optimal with **SACR-IPTZ** as the PC, yielding 99% of **1** (Table 8, entry 8).[39] The reaction does not readily proceed in toluene, yielding only 10% product, while in DMSO an increase in the yield (64% of **1**) compared to that in DCM is observed, ostensibly due to a partial suppression of the

Table 7 Energy transfer-mediated Ni-catalyzed cross-coupling esterification[a]

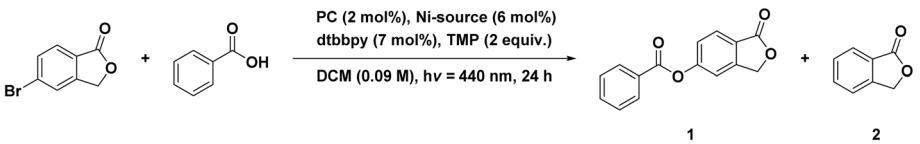


| Entry | Photocatalyst | Conditions | Yield **1**/% | Yield **2**/% |
|---|---|---|---|---|
| 1 | None | Ni(COD)$_2$ | 10 ± 1 | 11 ± 2 |
| 2 | None | NiBr$_2$·glyme | 0 ± 0 | 0 ± 0 |
| 3 | **DiICztBu$_4$** | Ni(COD)$_2$ | 59 ± 2 | 28 ± 0 |
| 4 | **DiICztBu$_4$** | NiBr$_2$·glyme | 31 ± 4 | 15 ± 1 |
| 5 | **DiICzMes$_4$** | Ni(COD)$_2$ | 65 ± 4 | 28 ± 3 |
| 6 | **DiICzMes$_4$** | NiBr$_2$·glyme | 41 ± 0 | 19 ± 1 |
| 7 | **DiICzMes$_4$** | [Ni(dtbbpy)(OH$_2$)$_4$]Cl$_2$ | 68 ± 1 | 18 ± 0 |
| 8 | **DiICztBuCz$_4$** | Ni(COD)$_2$ | 60 ± 6 | 31 ± 2 |
| 9 | **DiICztBuCz$_4$** | NiBr$_2$·glyme | 20 ± 1 | 20 ± 1 |
| 10 | **DiICztBuDPA$_4$** | Ni(COD)$_2$ | 47 ± 5 | 14 ± 2 |
| 11 | **DiICztBuDPA$_4$** | NiBr$_2$·glyme | 27 ± 3 | 11 ± 0 |
| 12 | **4CzIPN** | Ni(COD)$_2$ | 43 ± 2 | 36 ± 4 |
| 13 | **4CzIPN** | NiBr$_2$·glyme | 31 ± 0 | 19 ± 0 |
| 14 | ***fac*-Ir(ppy)$_3$** | Ni(COD)$_2$ | 65 ± 1 | 15 ± 1 |
| 15 | ***fac*-Ir(ppy)$_3$** | NiBr$_2$·glyme | 49 ± 5 | 16 ± 1 |

[a] 5-Bromophthalide (0.188 mmol, 1.0 equiv.), benzoic acid (0.301 mmol, 1.6 equiv.), 2,2,6,6-tetramethylpiperidine (TMP) (0.375 mmol, 2.0 equiv.), Ni source (0.011 mmol, 6 mol%), 4,4′-di-*tert*-butyl-2,2′-bipyridine (dtbbpy) (0.013 mmol, 7 mol%) and PC (0.004 mmol, 2 mol%) in DCM (0.09 M). Yields were determined by $^1$H NMR spectroscopy using 1,3,5-trimethoxybenzene as the internal standard.

Table 8 Reaction optimization of the Ni-co-catalyzed cross-coupling esterification reaction[a]

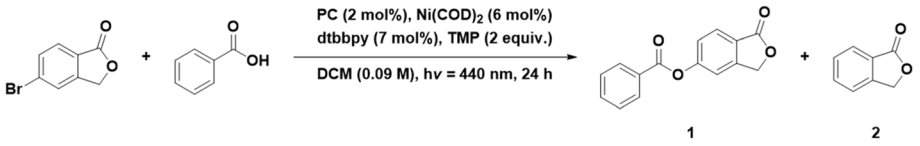


| Entry | Solvent | PC | Conditions | Yield **1**/% | Yield **2**/% |
|---|---|---|---|---|---|
| 1 | DCM | **DiICzMes$_4$** | Ni(COD)$_2$ | 60 ± 3 | 30 ± 1 |
| 2 | Toluene | **DiICzMes$_4$** | Ni(COD)$_2$ | 10 ± 3 | — |
| 3 | DMSO | **DiICzMes$_4$** | Ni(COD)$_2$ | 64 ± 5 | 21 ± 1 |
| 4 | DMSO : toluene 1 : 1 | **DiICzMes$_4$** | Ni(COD)$_2$ | 74 ± 2 | 15 ± 1 |
| 5 | DMSO : toluene 1 : 1 | **DiICzMes$_4$** | Ni(COD)$_2$, 3 h | 54 ± 0 | 13 ± 0 |
| 6 | DMSO : toluene 1 : 1 | ***fac*-Ir(ppy)$_3$** | Ni(COD)$_2$ | 77 ± 1 | 15 ± 0 |
| 7 | DMSO : toluene 1 : 1 | ***fac*-Ir(ppy)$_3$** | Ni(COD)$_2$, 3 h | 68 ± 2 | 16 ± 2 |
| 8 | DMSO : toluene 1 : 1 | **DiICzMes$_4$** | [Ni(dtbbpy)(H$_2$O)$_4$]Cl$_2$ | 81 ± 1 | 13 ± 1 |
| 9 | DMSO : toluene 1 : 1 | **SACR-IPTZ**[b] | Ni(COD)$_2$ | 99 | — |

[a] 5-Bromophthalide (0.188 mmol, 1.0 equiv.), benzoic acid (0.301 mmol, 1.6 equiv.), TMP (0.375 mmol, 2.0 equiv.), Ni-source (0.011 mmol, 6 mol%), dtbbpy (0.013 mmol, 7 mol%) and PC (0.004 mmol, 2 mol%) in the respective solvent (0.09 M). Yields were determined by $^1$H NMR spectroscopy using 1,3,5-trimethoxybenzene as the internal standard. [b] Literature yield taken from ref. 39 5-bromophthalide (0.188 mmol, 1.0 equiv.), benzoic acid (0.301 mmol, 1.6 equiv.), TMP (0.375 mmol, 2.0 equiv.), Ni-source (0.011 mmol, 6 mol%), dtbbpy (0.013 mmol, 7 mol%) and PC (0.004 mmol, 2 mol%) in the respective solvent (0.09 M), $\lambda_{exc}$ = 400 nm.

formation of **2** (Table 8, entry 1–3). Using 1 : 1 DMSO : toluene in combination with the preformed Ni complex [Ni(dtbbpy)(OH$_2$)$_4$]Cl$_2$ and **DiICzMes$_4$** as the PC resulted in 81% yield of **1** and only 13% of **2** (Table 8, entry 7). Reducing the reaction time from 24 to 3 h resulted in a lower yield of **1** (54%) but not of **2** (13%) (Table 8, entry 5), while with ***fac*-Ir(ppy)$_3$** as the PC the product was obtained in 68% yield after 3 h (Table 8, entry 7). While the reaction with ***fac*-Ir(ppy)$_3$** is slightly faster than with **DiICzMes$_4$**, effectively similar yields of 74 and 77% were obtained after 24 h using **DiICzMes$_4$** and ***fac*-Ir(ppy)$_3$**, respectively.

## Conclusion

We have investigated four DiICz emitters as fast and efficient DET photocatalysts in five different energy transfer reactions, highlighting their ability to activate high triplet energy substrates and outperform literature reference PCs. There is scant solvent dependency of the $T_1$ state energies of these four MR-TADF PCs, unlike D–A TADF PCs such as **4CzIPN**. Surprisingly, we observed a dependency of the sensitivity of $O_2$ quenching as a competitive triplet quencher as a function of the nature of the PEnT reaction, even when the $E_T$ of the substrate was the same. Reactions that proceed sufficiently rapidly with these PCs show little to no $O_2$ dependency on the final yield, which is a benefit of these compounds as photocatalysts. This suggests that the quenching of the excited state by $O_2$ is not competitive with the DET kinetics to the substrate. Excitingly, DET to substrates with triplet energies as high as 3.0 eV is feasible with **DiICztBu$_4$** and **DiICzMes$_4$**, both of which catalyze the sigmatropic shift of (*S*)-verbenone, yielding the product in around 38% yield. We concluded that there is no connection between either the yield or the reaction rate and the $\Delta E_{ST}$ of the PC. This study reveals the particularly valuable and wide utility of **DiCzMes$_4$** as a PEnT photocatalyst for substrates possessing high triplet energies.

## Author contributions

E. Z.-C. conceived and managed the project and supervised the work. D. H. synthesized **DiICzMes$_4$** and **DiICztBuCz$_4$**, E. B. synthesized **DiICztBuDPA$_4$** and L. H. synthesized **DiICztBu$_4$**. D. H. performed the steady-state emission and absorption measurements in toluene, T. H. measured the photoluminescence quantum yields of the four photocatalysts, and the emission lifetimes of the photocatalysts in presence of cinnamyl acetate, and L. H. performed steady-state emission and absorption measurements in DCM, DMF and EtOAc, the time-resolved photoluminescence measurements in DCM, and the determination of $\Delta E_{ST}$ in 2-MeTHF. L. H. carried out photocatalysis reactions and photostability studies. L. H., D. H. and E. Z.-C. contributed to the manuscript writing and discussion.

## Conflicts of interest

The authors declare no competing interests.

## Data availability

The research data supporting this publication can be accessed at **https://doi.org/10.17630/22609279-98d6-4d3c-a1c1-b1f14b04b22d**. Supplementary information: synthetic procedures, UV-vis absorption and photoluminescence spectra (room temperature steady-state, 77 K steady-state, and 77 K gated emission), time-resolved PL decays, photoluminescence

quantum yield data, photocatalysis procedures, and photostability studies. See DOI: https://doi.org/10.1039/d5sc04014k.

## Acknowledgements

We thank the European Union H2020 research and innovation program for the funding under the Marie S. Curie Grant Agreement (PhotoReAct, No. 956324). We thank Geena Zoubarev for the contribution to the initial photocatalytic assessments. We thank Dr Megan Bryden, Francis Millward, and Violaine Manet for providing samples of **4CzIPN** and ***fac*-Ir(ppy)$_3$**. We thank EPSRC for financial support (EP/W522259/1, EP/W007517/1 and EP/M02105X/1).

## References

1 S. Dutta, J. E. Erchinger, F. Strieth-Kalthoff, R. Kleinmans and F. Glorius, Energy transfer photocatalysis: exciting modes of reactivity, *Chem. Soc. Rev.*, 2024, **53**, 1068–1089.
2 T. Neveselý, M. Wienhold, J. J. Molloy and R. Gilmour, Advances in the E → Z Isomerization of Alkenes Using Small Molecule Photocatalysts, *Chem. Rev.*, 2022, **122**, 2650–2694.
3 J. Großkopf, T. Kratz, T. Rigotti and T. Bach, Enantioselective Photochemical Reactions Enabled by Triplet Energy Transfer, *Chem. Rev.*, 2022, **122**, 1626–1653.
4 M. Tabachnyk, B. Ehrler, S. Gelinas, M. L. Bohm, B. J. Walker, K. P. Musselman, N. C. Greenham, R. H. Friend and A. Rao, Resonant energy transfer of triplet excitons from pentacene to PbSe nanocrystals, *Nat. Mater.*, 2014, **13**, 1033–1038.
5 F. Strieth-Kalthoff, M. J. James, M. Teders, L. Pitzer and F. Glorius, Energy transfer catalysis mediated by visible light: principles, applications, directions, *Chem. Soc. Rev.*, 2018, **47**, 7190–7202.
6 J. B. Metternich and R. Gilmour, A Bio-Inspired, Catalytic E → Z Isomerization of Activated Olefins, *J. Am. Chem. Soc.*, 2015, **137**, 11254–11257.
7 B. Kweon, L. Blank, J. Soika, A. Messara, C. G. Daniliuc and R. Gilmour, Regio- and Stereo-Selective Isomerization of Borylated 1,3-Dienes Enabled by Selective Energy Transfer Catalysis, *Angew. Chem., Int. Ed.*, 2024, **63**, e202404233.
8 X. Zhang and T. Rovis, Photocatalyzed Triplet Sensitization of Oximes Using Visible Light Provides a Route to Nonclassical Beckmann Rearrangement Products, *J. Am. Chem. Soc.*, 2021, **143**, 21211–21217.
9 Z. Lu and T. P. Yoon, Visible Light Photocatalysis of [2+2] Styrene Cycloadditions by Energy Transfer, *Angew. Chem., Int. Ed.*, 2012, **51**, 10329–10332.
10 R. Alonso and T. Bach, A Chiral Thioxanthone as an Organocatalyst for Enantioselective [2+2] Photocycloaddition Reactions Induced by Visible Light, *Angew. Chem., Int. Ed.*, 2014, **53**, 4368–4371.
11 K. A. Rykaczewski and C. S. Schindler, Visible-Light-Enabled Paternò–Büchi Reaction via Triplet Energy Transfer for the Synthesis of Oxetanes, *Org. Lett.*, 2020, **22**, 6516–6519.
12 D. R. Heitz, J. C. Tellis and G. A. Molander, Photochemical Nickel-Catalyzed C–H Arylation: Synthetic Scope and Mechanistic Investigations, *J. Am. Chem. Soc.*, 2016, **138**, 12715–12718.
13 E. R. Welin, C. Le, D. M. Arias-Rotondo, J. K. McCusker and D. W. C. MacMillan, Photosensitized, energy transfer-mediated organometallic catalysis through electronically excited nickel(II), *Science*, 2017, **355**, 380–385.
14 S. Wang, P. Ma, S. Shaik and H. Chen, Valence-Inverted States of Nickel(II) Complexes Perform Facile C–H Bond Activation, *J. Am. Chem. Soc.*, 2022, **144**, 14607–14613.
15 E. Brachet, T. Ghosh, I. Ghosh and B. König, Visible light C–H amidation of heteroarenes with benzoyl azides, *Chem. Sci.*, 2015, **6**, 987–992.
16 M. Teders, C. Henkel, L. Anhäuser, F. Strieth-Kalthoff, A. Gómez-Suárez, R. Kleinmans, A. Kahnt, A. Rentmeister, D. Guldi and F. Glorius, The energy-transfer-enabled biocompatible disulfide–ene reaction, *Nat. Chem.*, 2018, **10**, 981–988.
17 J. Majhi, R. K. Dhungana, Á. Rentería-Gómez, M. Sharique, L. Li, W. Dong, O. Gutierrez and G. A. Molander, Metal-Free Photochemical Imino-Alkylation of Alkenes with Bifunctional Oxime Esters, *J. Am. Chem. Soc.*, 2022, **144**, 15871–15878.
18 W. G. Herkstroeter, A. A. Lamola and G. S. Hammond, Mechaisms of photochemical reactions in solution. XXVIII. 1 Values of triplet excitation energies of selected sensitizers, *J. Am. Chem. Soc.*, 1964, **86**, 4537–4540.
19 A. Köhler and H. Bässler, Triplet states in organic semiconductors, *Mater. Sci. Eng., R*, 2009, **66**, 71–109.
20 C. M. Marian, Understanding and Controlling Intersystem Crossing in Molecules, *Annu. Rev. Phys. Chem.*, 2021, **72**, 617–640.
21 K. Kalyanasundaram, Photophysics, photochemistry and solar energy conversion with tris(bipyridyl)ruthenium(II) and its analogues, *Coord. Chem. Rev.*, 1982, **46**, 159–244.
22 A. Juris, V. Balzani, P. Belser and A. von Zelewsky, Characterization of the Excited State Properties of Some New Photosensitizers of the Ruthenium (Polypyridine) Family, *Helv. Chim. Acta*, 1981, **64**, 2175–2182.
23 M. S. Lowry, J. I. Goldsmith, J. D. Slinker, R. Rohl, R. A. Pascal, G. G. Malliaras and S. Bernhard, Single-Layer Electroluminescent Devices and Photoinduced Hydrogen Production from an Ionic Iridium(III) Complex, *Chem. Mater.*, 2005, **17**, 5712–5719.
24 J. M. Dos Santos, D. Hall, B. Basumatary, M. Bryden, D. Chen, P. Choudhary, T. Comerford, E. Crovini, A. Danos, J. De, S. Diesing, M. Fatahi, M. Griffin, A. K. Gupta, H. Hafeez, L. Hämmerling, E. Hanover, J. Haug, T. Heil, D. Karthik, S. Kumar, O. Lee, H. Li, F. Lucas, C. F. R. Mackenzie, A. Mariko, T. Matulaitis, F. Millward, Y. Olivier, Q. Qi, I. D. W. Samuel, N. Sharma, C. Si, L. Spierling, P. Sudhakar, D. Sun, E. Tankelevičiūtė, M. Duarte Tonet, J. Wang, T. Wang, S. Wu, Y. Xu, L. Zhang and E. Zysman-Colman, The Golden Age of Thermally Activated Delayed Fluorescence Materials: Design and Exploitation, *Chem. Rev.*, 2024, **124**, 13736–14110.

25 J. Luo and J. Zhang, Donor–Acceptor Fluorophores for Visible-Light-Promoted Organic Synthesis: Photoredox/Ni Dual Catalytic C(sp3)–C(sp2) Cross-Coupling, *ACS Catal.*, 2016, **6**, 873–877.
26 M. A. Bryden and E. Zysman-Colman, Organic thermally activated delayed fluorescence (TADF) compounds used in photocatalysis, *Chem. Soc. Rev.*, 2021, **50**, 7587–7680.
27 E. Zysman-Colman, Molecular designs offer fast exciton conversion, *Nat. Protoc.*, 2020, **14**, 593–594.
28 Y. Tsuchiya, S. Diesing, F. Bencheikh, Y. Wada, P. L. dos Santos, H. Kaji, E. Zysman-Colman, I. D. W. Samuel and C. Adachi, Exact Solution of Kinetic Analysis for Thermally Activated Delayed Fluorescence Materials, *J. Phys. Chem. A*, 2021, **125**, 8074–8089.
29 G. Meng, H. Dai, Q. Wang, J. Zhou, T. Fan, X. Zeng, X. Wang, Y. Zhang, D. Yang, D. Ma, D. Zhang and L. Duan, High-efficiency and stable short-delayed fluorescence emitters with hybrid long- and short-range charge-transfer excitations, *Nat. Commun.*, 2023, **14**, 2394.
30 A. R. Meyer, M. V. Popescu, A. Sau, N. H. Damrauer, R. S. Paton and T. P. Yoon, Combined Synthetic, Spectroscopic, and Computational Insights Into a General Method for Photosensitized Alkene Aziridination, *ACS Catal.*, 2024, **14**, 12310–12317.
31 J. Lu, B. Pattengale, Q. Liu, S. Yang, W. Shi, S. Li, J. Huang and J. Zhang, Donor-Acceptor Fluorophores for Energy-Transfer-Mediated Photocatalysis, *J. Am. Chem. Soc.*, 2018, **140**, 13719–13725.
32 $E_T$ measured at 77 K in 2-MeTHF glass from the gated emission acquired in a time window of 1–9 ms after excitation.
33 H. J. Timpe, K. P. Kronfeld, U. Lammel, J. P. Fouassier and D. J. Lougnot, Excited states of ketones as electron donors—ketone—iodonium salt systems as photoinitiators for radical polymerization, *J. Photochem. Photobiol., A*, 1990, **52**, 111–122.
34 M. A. Bryden, F. Millward, T. Matulaitis, D. Chen, M. Villa, A. Fermi, S. Cetin, P. Ceroni and E. Zysman-Colman, Moving Beyond Cyanoarene Thermally Activated Delayed Fluorescence Compounds as Photocatalysts: An Assessment of the Performance of a Pyrimidyl Sulfone Photocatalyst in Comparison to 4CzIPN, *J. Org. Chem.*, 2023, **88**, 6364–6373.
35 S. Sharma and S. Sengupta, Twisted organic TADF triads based on a diindolocarbazole donor for efficient photoisomerization of stilbene and photo-arylation of heteroarenes, *Org. Chem. Front.*, 2023, **10**, 6087–6095.
36 G. S. Hammond, J. Saltiel, A. A. Lamola, N. J. Turro, J. S. Bradshaw, D. O. Cowan, R. C. Counsell, V. Vogt and C. Dalton, Mechanisms of photochemical reactions in solution. XXII. 1 Photochemical cis-trans isomerization, *J. Am. Chem. Soc.*, 1964, **86**, 3197–3217.
37 M. Yokoyama, K. Inada, Y. Tsuchiya, H. Nakanotani and C. Adachi, Trifluoromethane modification of thermally activated delayed fluorescence molecules for high-efficiency blue organic light-emitting diodes, *Chem. Commun.*, 2018, **54**, 8261–8264.
38 E. R. Sauvé, D. M. Mayder, S. Kamal, M. S. Oderinde and Z. M. Hudson, An imidazoacridine-based TADF material as an effective organic photosensitizer for visible-light-promoted [2 + 2] cycloaddition, *Chem. Sci.*, 2022, **13**, 2296–2302.
39 R. Hojo, K. Bergmann, S. A. Elgadi, D. M. Mayder, M. A. Emmanuel, M. S. Oderinde and Z. M. Hudson, Imidazophenothiazine-Based Thermally Activated Delayed Fluorescence Materials with Ultra-Long-Lived Excited States for Energy Transfer Photocatalysis, *J. Am. Chem. Soc.*, 2023, **145**, 18366–18381.
40 S. Madayanad Suresh, D. Hall, D. Beljonne, Y. Olivier and E. Zysman-Colman, Multiresonant Thermally Activated Delayed Fluorescence Emitters Based on Heteroatom-Doped Nanographenes: Recent Advances and Prospects for Organic Light-Emitting Diodes, *Adv. Funct. Mater.*, 2020, **30**, 1908677.
41 C. Prentice, J. Morrison, A. D. Smith and E. Zysman-Colman, Multi-Resonant Thermally Activated Delayed Fluorescent (MR-TADF) Compounds as Photocatalysts, *Chem.–Eur. J.*, 2023, **29**, e202202998.
42 L. Hämmerling and E. Zysman-Colman, Building a photocatalyst library of MR-TADF compounds with tunable excited-state redox potentials, *Chem Catal.*, 2024, **4**, 101061.
43 V. V. Patil, H. L. Lee, I. Kim, K. H. Lee, W. J. Chung, J. Kim, S. Park, H. Choi, W.-J. Son, S. O. Jeon and J. Y. Lee, Purely Spin-Vibronic Coupling Assisted Triplet to Singlet Up-Conversion for Real Deep Blue Organic Light-Emitting Diodes with Over 20% Efficiency and y Color Coordinate of 0.05, *Adv. Sci.*, 2021, **8**, 2101137.
44 D. Hall, K. Stavrou, E. Duda, A. Danos, S. Bagnich, S. Warriner, A. M. Z. Slawin, D. Beljonne, A. Köhler, A. Monkman, Y. Olivier and E. Zysman-Colman, Diindolocarbazole – achieving multiresonant thermally activated delayed fluorescence without the need for acceptor units, *Mater. Horiz.*, 2022, **9**, 1068–1080.
45 H. L. Lee, S. O. Jeon, I. Kim, S. C. Kim, J. Lim, J. Kim, S. Park, J. Chwae, W.-J. Son, H. Choi and J. Y. Lee, Multiple-Resonance Extension and Spin-Vibronic-Coupling-Based Narrowband Blue Organic Fluorescence Emitters with Over 30% Quantum Efficiency, *Adv. Mater.*, 2022, **34**, 2202464.
46 V. V. Patil, J. Lim, S. M. Cho and J. Y. Lee, Highly Efficient C/N-Fused Architecture for Narrowband Deep-Blue Thermally Activated Delayed Fluorescence, *Adv. Opt. Mater.*, 2024, **12**, 2300551.
47 J. Kang, S. O. Jeon, I. Kim, H. L. Lee, J. Lim and J. Y. Lee, Color Stable Deep Blue Multi-Resonance Organic Emitters with Narrow Emission and High Efficiency, *Adv. Sci.*, 2023, **10**, 2302619.
48 J. H. Lee, T. Watanabe, L. Hartmann and T. Yasuda, Blue-to-Green Fine-Tunable Narrowband Delayed Fluorescence in Peripherally Dendritic Modified Bis-Indolocarbazoles, *Angew. Chem., Int. Ed.*, 2025, **64**, e202505191, DOI: **10.1002/anie.202505191**.
49 M. A. Bryden, F. Millward, O. S. Lee, L. Cork, M. C. Gather, A. Steffen and E. Zysman-Colman, Lessons learnt in

photocatalysis – the influence of solvent polarity and the photostability of the photocatalyst, *Chem. Sci.*, 2024, **15**, 3741–3757.

50 D. K. A. Phan Huu, S. Saseendran and A. Painelli, Effective models for TADF: the role of the medium polarizability, *J. Mater. Chem. C*, 2022, **10**, 4620–4628.

51 L. Schmid, C. Kerzig, A. Prescimone and O. S. Wenger, Photostable Ruthenium(II) Isocyanoborato Luminophores and Their Use in Energy Transfer and Photoredox Catalysis, *JACS Au*, 2021, **1**, 819–832.

52 L. Schmid, F. Glaser, R. Schaer and O. S. Wenger, High Triplet Energy Iridium(III) Isocyanoborato Complex for Photochemical Upconversion, Photoredox and Energy Transfer Catalysis, *J. Am. Chem. Soc.*, 2022, **144**, 963–976.

53 K. E. Jones, B. Park, N. A. Doering, M.-H. Baik and R. Sarpong, Rearrangements of the Chrysanthenol Core: Application to a Formal Synthesis of Xishacorene B, *J. Am. Chem. Soc.*, 2021, **143**, 20482–20490.